



Estimating above ground biomass of winter wheat at early growth stages using digital images and deep convolutional neural network



Juncheng Ma^a, Yunxia Li^b, Yunqiang Chen^b, Keming Du^{a,*}, Feixiang Zheng^a, Lingxian Zhang^b, Zhongfu Sun^a

^a Institute of Environment and Sustainable Development in Agriculture, Chinese Academy of Agricultural Sciences, Beijing, 100081, China

^b College of Information and Electrical Engineering, China Agricultural University, Beijing, 100083, China

ARTICLE INFO

Keywords:

Winter wheat
Above ground biomass
RGB images
Deep convolutional neural network

ABSTRACT

Above ground biomass (AGB) is a critical trait indicating the growth of winter wheat. Currently, non-destructive methods for measuring AGB heavily depend on tools such as Remote Sensing and LiDAR, which is subject to specialized knowledge and high-cost. Low-cost solutions appear therefore to be a necessary supplement. In this study, an easy-to-use AGB estimation method for winter wheat at early growth stages was proposed by using digital images captured under field conditions and Deep Convolutional Neural Network (DCNN). Using canopy images as input, the DCNN was trained to learn the relationship between the canopy and the corresponding AGB. To compare the results of the DCNN, conventionally adopted methods for estimating AGB in conjunction with some color and texture feature extraction techniques were used. Results showed strong correlations could be observed between the actual measurements of AGB to those estimated by the DCNN, with high coefficient of determination ($R^2 = 0.808$) and low Root-Mean-Square-Error (RMSE = 0.8913 kg/plot, NRMSE = 24.95%). Factors may influence the accuracy of the DCNN were evaluated. Results showed selecting suitable values of these factors for the DCNN was the guarantee to accurate estimation results. Plant density was proved to be an influence of factor to all the estimation methods based on digital images. The performances of all the methods were influenced to varying degrees while the DCNN achieved the best robustness, indicating the DCNN with RGB images could be an efficient and robust tool for estimating AGB of winter wheat at early growth stages.

1. Introduction

Above ground biomass (AGB) is one of the most commonly used traits indicating the growth of winter wheat (Eitel et al., 2014; Schirrmann et al., 2016b; Walter et al., 2018; Zhang et al., 2018). It is of great practical significance to monitor the growth and to estimate the yield. The conventional methods involving destructive sampling and manual calculation of the dry weight to measure AGB is prohibitively time consuming and laborious (Casadesús and Villegas, 2014; Walter et al., 2018; Zhang et al., 2018). Due to the limitations, the conventional methods can only process a limited amount of data, making it impossible to be used in high-throughput plant phenotyping tasks.

With the development of field-based plant phenotyping, many non-destructive methods for measuring AGB were proposed. A common way to estimate AGB of winter wheat was through the estimation of vegetation indices (VIs) and regression analysis. VIs can be calculated from light reflected at different wavelengths from images captured by

Remote Sensing (RS) or ground-based image sensors (Pöölön et al., 2013; Jannoura et al., 2015; Liebisch et al., 2015; Rasmussen et al., 2016; Zhang et al., 2018). The normalized difference vegetation index (NDVI) was the most widely used VIs on estimating AGB, which was defined as the ratio of the reflectance in the near-infrared and red channel of the spectrum (Tucker, 1979). Strong correlations between NDVI and ground measured biomass of crop can be observed (Pöölön et al., 2013; Rasmussen et al., 2016; Schirrmann et al., 2016b). Except for NDVI, some other VIs were also successfully adopted to estimate AGB, such as Modified Chlorophyll Absorption in Reflectance Index (MCARI) (Daughtry et al., 2000; Pöölön et al., 2013), the enhanced NDVI index (ENDVI) (Rasmussen et al., 2016), and GnyLi (GnyLi et al., 2014). With the increased use of low-cost Unmanned Aerial Vehicles (UAVs), VIs derived from low-cost UAV imagery were able to achieve good estimation of AGB, such as Normalized Green-Red Difference Index (NGRDI) (Jannoura et al., 2015; Rasmussen et al., 2016), Excess Green (ExG) (Rasmussen et al., 2016; Schirrmann et al., 2016a;

* Corresponding author at: Institute of Environment and Sustainable Development in Agriculture, Chinese Academy of Agricultural Sciences, 12, Zhongguancun South Street, Haidian District, Beijing, 100081, China.

E-mail address: dukeming@caas.cn (K. Du).

Woebecke et al., 1995), RGB vegetation index (RGBVI) (Possoch et al., 2016). While the VIs showed excellent ability to estimate AGB, there were still limitations that the VIs can be affected by saturation of the index (Eitel et al., 2014; Tucker, 1977; Walter et al., 2018). Canopy height is another widely used parameter to estimate AGB. Schirrmann et al. (2016) showed that the inclusion of plant height into the model, established to estimate AGB by plant coverage, could efficiently increase the estimation accuracy. They also revealed plant height alone was a strong predictor of AGB. The same conclusions can be observed in Bendig et al. (2015); Pittman et al. (2015), and Walter et al. (2018). Many methods have been used to obtain plant height data, such as Light Detection And Ranging (LiDAR) (Eitel et al., 2014; Pittman et al., 2015), ultrasonic sensor (Chang et al., 2017; Moeckel et al., 2017; Pittman et al., 2015), UAVs (Bendig et al., 2015). However, these sensors were costly and required specialized knowledge, leading to low flexibility.

Ground-based images captured by low-cost devices can be an alternative to the expensive sensors and have received great interest. Many researchers have used ground-based images to estimate growth-related traits, such as Leaf Area Index (LAI) (Casadesús and Villegas, 2014; Fan et al., 2017), AGB (Casadesús and Villegas, 2014; Chung et al., 2017; Walter et al., 2018), plant height (Jiang et al., 2016; Walter et al., 2018). While ground-based images is a promising way to estimate growth-related traits, a more feasible and robust approach should be explored.

The objective of this study was to apply the Deep Convolutional Neural Network (DCNN) to the estimation of AGB for winter wheat at early growth stages using ground-based digital images. The DCNN was used to model the relationship between an RGB image of winter wheat canopy in a specific area and the corresponding AGB. By following the proposed framework including canopy images processing, image augmentation, construction of the DCNN, this paper investigated the potential of the DCNN using ground-based digital images in estimating AGB of winter wheat at early growth stages.

2. Materials and methods

2.1. Experiment setup

The experiment took place in the field station of Shangqiu Academy of Agriculture and Forestry Sciences in Shuangba, Henan, China (Lat: 34°32'21.1884": N, Long: 115°43'8.0868": E), which was located at the center of winter wheat producing areas of Huang-Huai Plain of China. The yearly average precipitation in this region was approximately 750 mm with an average temperature of 13 °C. The winter wheat cultivar was Guomai 301 which was one of the major wheat cultivars in China. Therefore, the winter wheat cultivar was adapted to the climate conditions. The plots were 5 m × 2.4 m. Plots (12) of winter wheat

were sown on 14th October 2017, with three target plant densities (120, 270 and 420 plants/m²) (Fig. 1). Each plant density was applied to four replicates. A total of 210 kg N ha⁻¹ was applied, of which 60% (126 kg N ha⁻¹) was used before sowing and 40% (84 kg N ha⁻¹) was used at early jointing stage. A total of 90 kg P ha⁻¹ and 45 kg K ha⁻¹ was applied before sowing.

2.2. Images collection and processing

It was important to maintain uniformity in the area under observation so that the amount of information used in each image was identical. A rectangle was laid down on the floor as a physical marker to ensure that all images contained to the same fraction of canopy (Fig. 1a). The color of the marker was white, and the size was 1 m × 1 m. With the growth of the winter wheat, the marker can be raised by putting sticks under the four corners. Three markers were placed within each plot, and a certain distance was kept between every two markers. The images were captured by a Canon EOS 600D digital camera which was mounted on a tripod (Fig. 1b). The camera oriented vertically downwards over the canopy at a distance of 1.5 m, resulting in a field of view of approximately seven rows of each plot. Images were taken at a focal length of 18 mm with an aperture of f/4. All images were obtained in a 5184 × 3456 pixel spatial resolution with flash always off and without optical or digital zoom. The images were captured between 10:00 am and 11:00 am and stored in JPG file format.

The image collection was performed 17 times from days after sowing (DAS) 44 to 153. A dataset containing 612 images (4 plots × 3 densities × 3 markers × 17 times) was constructed, which was then divided into three subsets, i.e., training, validation, and test datasets. The training dataset (4 plots × 3 densities × 2 markers × 17 times) contained two of the three marker images of each plot and the test dataset (4 plots × 3 densities × 1 markers × 17 times) contained the left one marker image of each plot. Of the images in training dataset, 20% was randomly chosen to construct validation dataset. Prior to image analysis, all the images were manually cropped to eliminate the parts outside the markers, which resulted in images in a 2763 × 2757 pixel spatial resolution. The image dataset for the DCNN was constructed by reshaping the cropped images into pixel size 64 × 64 (height × width). To enlarge the image dataset and decrease the chance of overfitting, a data augmentation scheme was adopted (Fig. 2).

The following augmentations were conducted: 90° rotation, 180° rotation, 270° rotation, horizontal flip, and vertical flip. In field conditions, illumination was the major influence of factors affecting image collection. Therefore, to make the DCNN robust to the illumination change of field environment, the datasets were further augmented by simulating the illumination change. The augmentation can be achieved by transferring the images to HSV color space and adjusting the V component (Xiong et al., 2017). The augmentation scheme was



Fig. 1. Experiment setup, (a) the markers within each plot; (b) the camera mounted on a tripod.

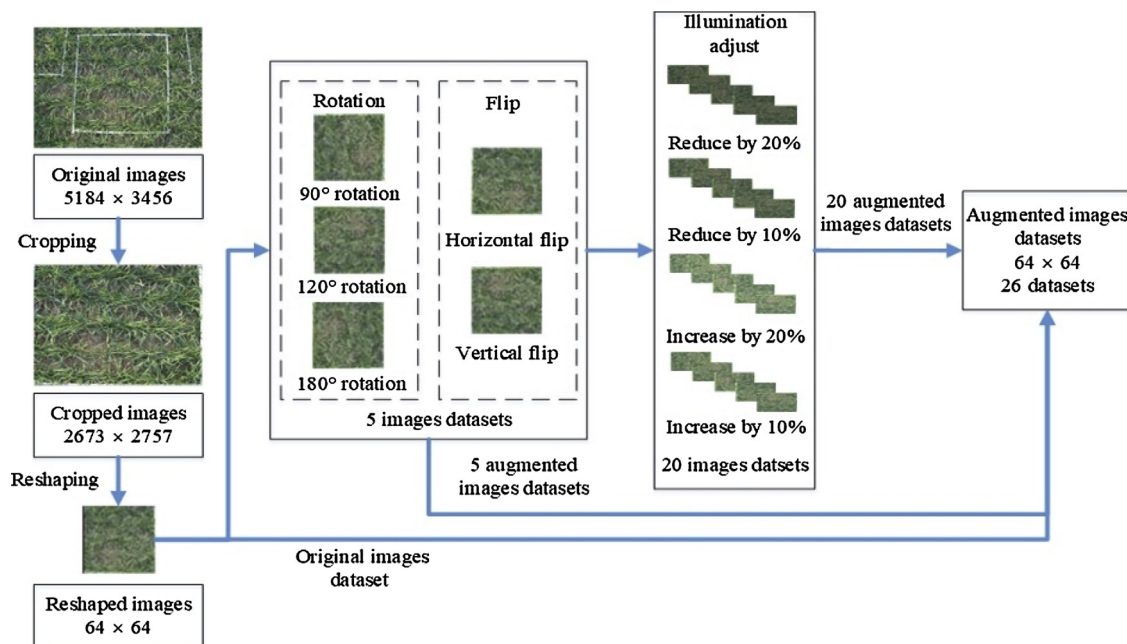


Fig. 2. Image processing scheme.

performed to the three subsets respectively, resulting in a dataset (the whole dataset) containing 15,912 images. The number of images in the three datasets was 8486, 2122, and 5304 respectively. Each image in the datasets was associated with an AGB value obtained by field measurement.

2.3. Above ground biomass measurement

Field measurements of AGB were performed simultaneously with image collection. These measurements were conducted at intervals ranging from three to eight days, specifically on DAS44, 48, 51, 55, 59, 65, 80, 93, 100, 109, 115, 133, 138, 143, 146, 150, and 153. For each measurement, five plants of winter wheat were randomly sampled in each plot outside of the markers. The measurement can be obtained by averaging the five dry weights and multiplying the corresponding plant density.

2.4. Deep convolutional neural network

The architecture of the DCNN used in this paper was depicted in Fig. 3. The DCNN consisted of four convolutional layers, four batch normalization layers, three pooling layers, and one fully connected layer. The input to the DCNN was an RGB image of winter wheat

canopy with size $64 \times 64 \times 3$, which would be mapped to a scalar AGB in the deeper layer of the DCNN. The convolutional layers used filters that had size 5×5 to extract features. The number of filters in each convolutional layer was 32, 64, 128, and 256 respectively, which was inspired by the VGGNet (Simonyan and Zisserman, 2014). Zero padding was not used by default except for the second convolutional layer so that the size of the feature maps in the deeper layer was as an integer. Following the convolutional layers were four batch normalization layers which can speed up network training and reduce the sensitivity to network initialization. The filters in pooling layers used in the DCNN had size 2×2 and stride 2, which had the effect of shrinking the feature maps by a factor of two. Instead of max pooling, the function used in the pooling layers was average pooling. Average pooling can be achieved by computing the average value of the kernel region. A fully connected layer with one hidden unit and a dropout layer with a dropout rate of 50% were used to reduce the dimensions of the feature maps down to a scalar. The output of the DCNN was the estimated AGB and mean-squared-error with the field measured value. The Rectified Linear Unit (ReLU) function was used as the activation function for all convolutional and fully connected layers (Krizhevsky et al., 2012; Ding and Taylor, 2016; Ghosal et al., 2018).

The DCNN was trained on a NVIDIA Quadro P4000 (8 GB memory) with CUDA 9.0. The stochastic gradient descent with momentum

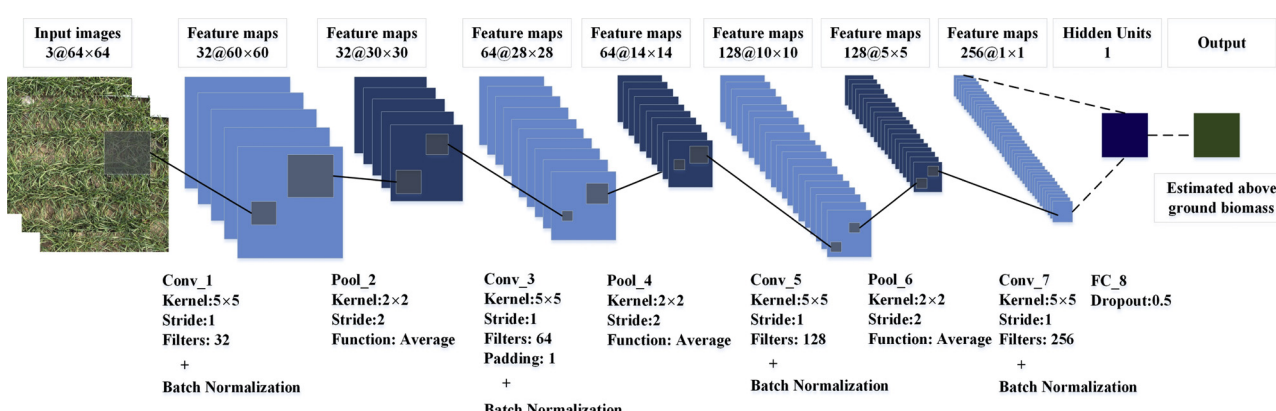


Fig. 3. Architecture of DCNN.

(SGDM) was used to optimize the network weights. The learning rate was initialized as 0.001 and dropped every 20 epochs by a drop factor of 0.1. The momentum was set to 0.9 and remained constant for the training process. A mini-batch of 64 was used. The maximum number of epochs used for training was set to 300.

2.5. Performance evaluation

Some influences of factors that may affect the performance of the DCNN on AGB estimation were evaluated so that the initial network architecture can be updated for better estimation results. These factors included the color information of canopy image, the amount of data augmentation, learning rate and mini-batch size. The other network parameters were kept fixed for the training process. In order to compare the performance of the DCNN, tests were performed with other estimating methods that have been adopted successfully to estimate AGB. It was reported that Canopy Cover (CC) had a strong correlation with AGB (Casadesús and Villegas, 2014; Bai et al., 2016; Baresel et al., 2017; Chung et al., 2017). Therefore, a linear regression model using CC as the predictor variable (LR-CC) was used as one of the compared methods. Besides, conventional classifiers in conjunction with some color and texture feature extraction techniques, including Random Forest (RF) (Breiman, 2001), Support Vector Machine Regression (SVR) (Clevers et al., 2007) and Back propagation Neural Network (BPNN) (Wang et al., 2016), were also used as the compared methods.

The canopy images of winter wheat were captured at early growth stages, resulting in the existence of pixels representing non-vegetation elements in these images, such as soil. Therefore, it was necessary to perform image segmentation of vegetation for the compared methods prior to feature extraction. The segmentation was achieved by Canopeo, as well as the calculation of CC value (Patrignani and Ochsner, 2015; Chung et al., 2017). Some examples were shown in Fig. 4. Canopeo was developed based on color ratios of red to green (R/G) and blue to green (B/G) and an excess green index (2G-R-B), which was capable of detecting CC at high speed. The green canopy can be segmented by the

following criteria:

$$R/G < P_1 \text{ and } B/G < P_2 \text{ and } 2G - R - B > P_3 \quad (1)$$

where P_1 , P_2 , and P_3 were parameters for the color ratios that were typically set to 0.95, 0.95, 20 by default. In this paper, the default values for the parameters were adopted to segment the canopy images.

For the conventional classifiers that were compared to the DCNN, feature extraction from the segmented vegetation images was performed prior to model construction. The color information of winter wheat canopy was obviously different from that of the background. Therefore, color features were adopted as the distinguishing features. The color features used in this paper consisted of the mean and variance of the 15 channels from five color spaces, including R, G, B from RGB color space, H, S, V, from HSV color space, H, S, I, from HSI color space, L, a*, b*, from CIEL*a*b* color space and Y, Cb, Cr from YCbCr color space. Texture features derived from the Gray-level co-occurrence matrix of each channel were used as well. The texture features included contrast, correlation, energy and homogeneity of the 15 channels. Based on the feature designs, a feature set containing 90 features was conducted.

Linear regression analysis was utilized to compare model accuracy. Root-Mean-Squared Error (RMSE), Normalized Root-Mean-Squared Error (NRMSE) (Rischbeck et al., 2016), and coefficient of determination (R^2) were used as the criterion for model evaluation. The NRMSE was obtained by dividing the RMSE by the mean estimated AGB.

3. Results of AGB estimation

3.1. Results on the whole dataset

The performance of the DCNN evaluated over the test dataset was shown in Fig. 5. Regression analysis suggested that the AGB values estimated from the canopy images of winter wheat in the test dataset had a good agreement with the corresponding AGB values derived from field measurements ($R^2 = 0.808$, RMSE = 0.8913 kg/plot, NRMSE =

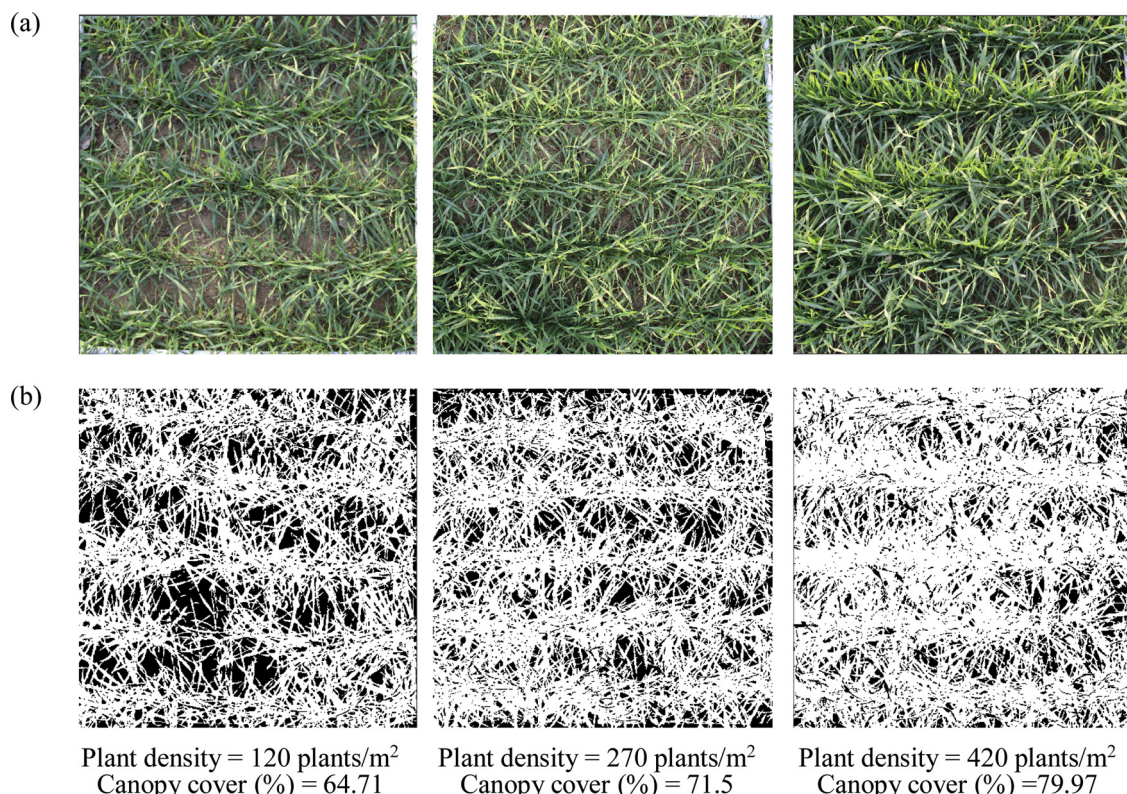


Fig. 4. Calculating CC using Canopeo, (a) Canopy images of different plant densities on DAS 44, (b) the segmentation results.

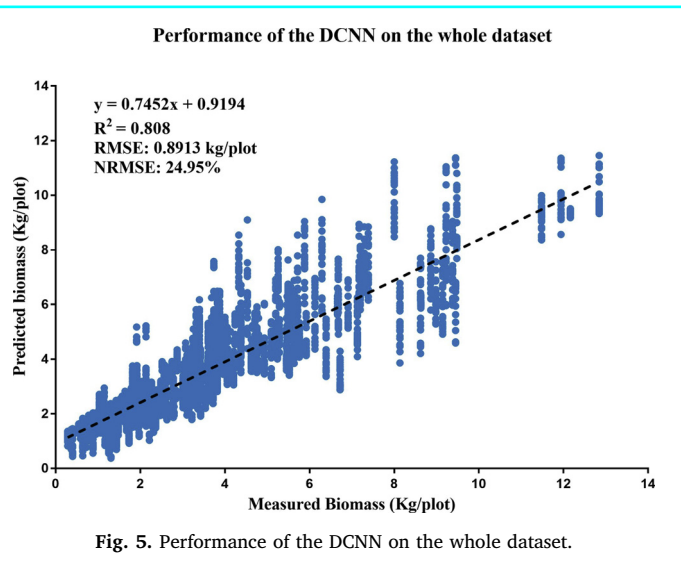


Fig. 5. Performance of the DCNN on the whole dataset.

24.95%).

The contributions of the color information of canopy images to AGB estimation were examined by constructing the gray whole dataset. The color information of images in the gray whole dataset was removed by transferring the color images to grayscale images. The DCNN was trained on the gray whole dataset, whose dimension of the images in the input layers was changed to one. The performance of the DCNN evaluated over the gray test dataset was shown in Fig. 6.

Compared to the performance on the whole dataset, the DCNN was obviously influenced by the absence of the color information. A degradation on the performance can be observed ($R^2 = 0.5857$, RMSE = 1.1872 kg/plot, NRMSE = 33.54%). The results indicated that the color information of canopy images made contributions to AGB estimation. The relationship between the measured and estimated AGB values was much clearer when the estimation results were demonstrated individually on each measured date (Fig. 7). The estimated AGB values by the DCNN on the whole dataset had strong relation to the measured values. It can be seen in Table 1 that the performance of the DCNN over the whole dataset had larger R^2 values compared to that over the gray whole dataset, as well as smaller errors, on each measured date.

The influence of the data augmentation scheme to the performance of the DCNN was evaluated by conducting experiments on the DCNN with datasets augmented by different augmentation methods. Five datasets were constructed, i.e., no augmentation, rotation + flip

augmentation, rotation + illumination adjustment augmentation, flip + illumination adjustment augmentation, and rotation + flip + illumination adjustment augmentation. R^2 , RMSE and NRMSE were adopted as the evaluation metrics. The estimation results were shown in Table 2. An obvious improvement on the performance of the DCNN by the data augmentation scheme can be observed. The DCNN over the five datasets had R^2 values equal to 0.2284, 0.4251, 0.5414, 0.7062 and 0.808, respectively, RMSE values equal to 1.9646, 1.5060, 1.3169, 1.1081 and 0.8913 kg/plot, respectively and NRMSE values equal to 56.38%, 52.31%, 42.45%, 32.15% and 24.95%.

The influence of learning rate to the performance of the DCNN was examined on the whole dataset with learning rate varying from 10^{-3} to 10^{-8} . The results were demonstrated in Table 2. It can be observed that the learning rate had a second-order effect on the performance of the DCNN. Although the DCNN reached the top ($R^2 = 0.7616$, RMSE = 0.8695 kg/plot, NRMSE = 25.64%) with the learning rate of 10^{-5} , the best performance was achieved by the DCNN with dynamic learning rate (Fig. 8a). The same method was utilized to evaluate the influence of mini-batch size to the performance of the DCNN. The range of the mini-batch size was varying from 8 to 256. The results were demonstrated in Table 2. Similar second-order effect on the performance of the DCNN can be observed for the influence of mini-batch size, indicating that the DCNN reached the top with the mini-batch size of 64 (Fig. 8b).

The capability of the DCNN to estimate AGB at late growth stages was evaluated by using images at jointing stage and booting stage. The late stage dataset was constructed by integrating the images of the two late stages to the whole dataset, resulting in 828 images, i.e. 612 for the early stages and 216 for the two late stages (4 plots \times 3 densities \times 3 markers \times 6 times). By following the same protocols for image processing as in the AGB estimation of early stages, the dataset was divided and augmented. The number of images in the three datasets was 11481, 2871, and 7176 respectively. The performance of the DCNN evaluated over the test dataset was shown in Fig. 9. Compared to the performance on the whole dataset, the DCNN evaluated over the late stage dataset gave worse results (Fig. 9a, $R^2 = 0.726$, RMSE = 1.557 Kg/plot, NRMSE = 26.10%). It can be seen that the R^2 value at the two late stages was much worse than that at early stages (Fig. 9b, $R^2 = 0.1328$, RMSE = 0.6241 Kg/plot, NRMSE = 6.06%), indicating that the DCNN in this study was not capable of estimating AGB at late growth stages.

According to the experiment setup, the CC values for each plot can be calculated by averaging the three CC values obtained from the three marker images within the plot. The CC dataset containing 204 observations (4 plots \times 3 densities \times 17 times) was constructed for the estimation of AGB, which was then divided into two subsets, i.e., calibration and test. 12 observations on DAS 115 were removed as outliers from the dataset due to strong illumination. The number of observations in the calibration and test datasets was 144 and 48 respectively. Linear regression analysis was then used to calibrate the model. The estimation results were shown in Fig. 10. The correlation ($R^2 = 0.7246$) can be observed between the field measurements and the predicted AGB. The RMSE was 0.9409 kg/plot and the NRMSE was 37.22%. Compared to the DCNN, LR-CC indicated worse R^2 and RMSE results on the whole dataset.

Prior to the development of the conventional classifiers, the correlation analysis was performed between pairs of parameters that included the 90 features and AGB measured from the field measurements (Table 3).

The features that were positively correlated to the AGB values were used to build the classifiers. It can be seen that the strongest correlations were observed between the texture features and the AGB measurements. Specifically, it was revealed that the energy of the six channels, i.e., H of HSV, L* of CIEL*a*b*, a* of CIEL*a*b*, b* of CIEL*a*b*, Cb of YCbCr and Cr of YCbCr ($r = 0.659^{**}$, 0.644^{**} , 0.669^{**} , 0.602^{**} , 0.594^{**} and 0.667^{**} , respectively), and the Homogeneity of a* of CIEL*a*b* channel ($r = 0.656^{**}$) had positive correlations with the AGB values. Therefore, these seven features were

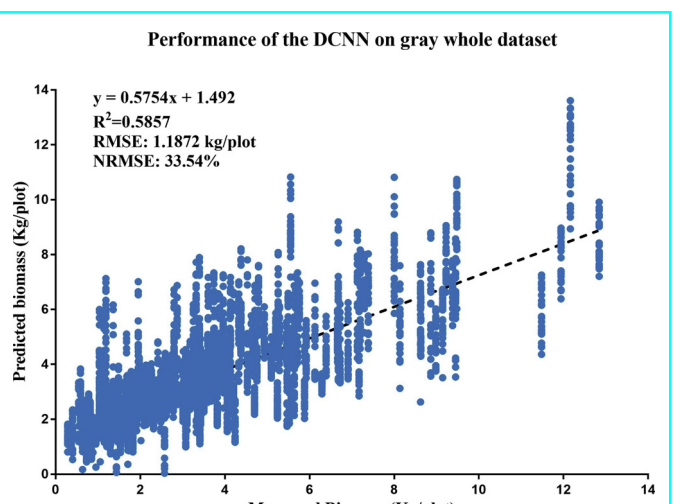


Fig. 6. Performance of the DCNN on the gray whole dataset.

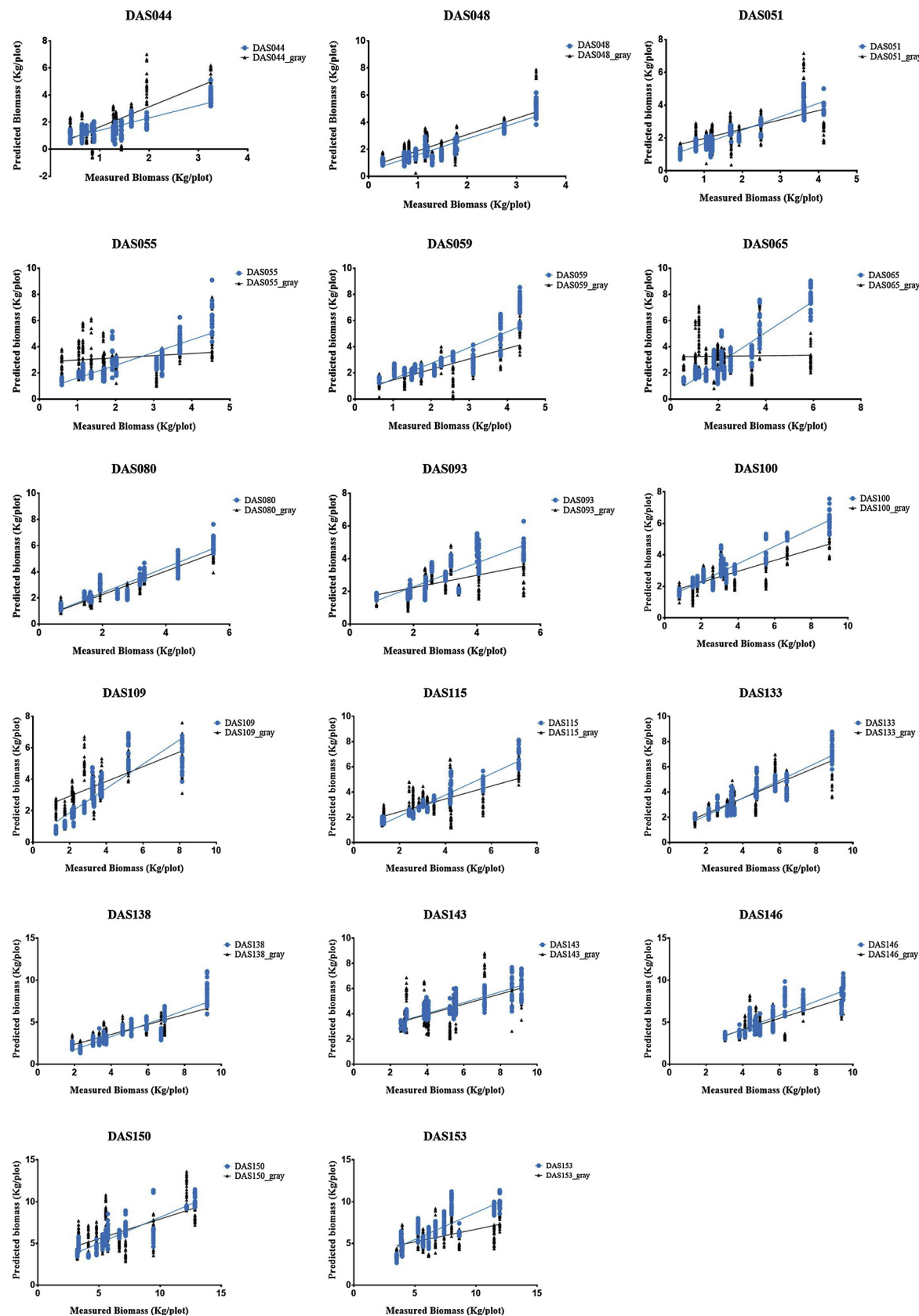


Fig. 7. Performance of the DCNN at each measured date.

Table 1
Estimation results of DCNN at each measured date.

Date	The whole dataset			Gray whole dataset		
	R ²	RMSE (kg/plot)	NRMSE (%)	R ²	RMSE (kg/plot)	NRMSE (%)
All dates	0.8080	0.8913	24.95%	0.5875	1.1872	33.54%
DAS044	0.7491	0.4908	29.34%	0.5857	0.9078	43.23%
DAS048	0.8211	0.4629	21.52%	0.6327	0.7646	31.25%
DAS051	0.8131	0.4623	18.77%	0.3914	0.8337	32.95%
DAS055	0.6777	0.7735	28.15%	0.0359	0.9863	30.98%
DAS059	0.7447	0.7603	25.95%	0.5443	0.7944	33.15%
DAS065	0.7950	0.8445	27.18%	0.0005	1.2800	39.02%
DAS080	0.8580	0.5199	17.76%	0.8639	0.4718	17.17%
DAS093	0.5972	0.7070	23.91%	0.2412	0.7922	30.69%
DAS100	0.8854	0.4527	14.02%	0.5588	0.7003	24.75%
DAS109	0.7501	0.7818	26.48%	0.4797	0.8566	23.91%
DAS115	0.8839	0.4989	15.10%	0.4126	0.9939	31.30%
DAS133	0.8073	0.6740	18.49%	0.6484	0.8968	24.76%
DAS138	0.7571	0.9178	23.93%	0.7026	0.8008	20.18%
DAS143	0.6726	0.6424	14.29%	0.3457	1.1920	27.11%
DAS146	0.7346	1.0070	18.19%	0.5501	1.2430	23.81%
DAS150	0.7937	0.9820	16.15%	0.3828	1.8460	29.01%
DAS153	0.6603	1.2370	18.49%	0.2650	1.3380	23.24%

used to build the conventional classifiers. The number of observations for the two datasets, i.e., train and test, was 144 and 48 respectively.

The estimation results by the conventional classifiers were shown in Fig. 11. The R² values of the conventional classifiers were 0.7796, 0.7445, and 0.736, respectively, the RMSE values were 0.9169, 0.9848, and 0.9379 kg/plot, respectively, and the NRMSE values were 35.19%, 51.85% and 34.36%, respectively. It was shown that the best performance was achieved by the RF classifier. Although there was a slight decrease in the R² values, the three conventional classifiers showed similar ability to LR-CC on estimating AGB, since these methods were based on the low-level features extracted from the digital images which were prone to be influenced by illumination and clutter background.

Table 4 presented the evaluation results of all the estimation methods on the whole dataset. It was revealed in Table 4 that the DCNN demonstrated superior results to the compared methods in the three metrics.

3.2. Results on the density datasets

According to the experiment setup, three datasets (Density 120, Density 270 and Density 450) corresponding to the three target plant

densities were constructed. Each dataset consisted of 1768 test images. The performance of the DCNN evaluated over the three density datasets were shown in Fig.12. Table 5 presented the statistics that assessed the performance.

It can be seen the DCNN for AGB estimation over the three density datasets had R² values equal to 0.8693, 0.8062, and 0.7433, respectively, RMSE values equal to 0.4796, 0.8495, and 1.1656 kg/plot, and NRMSE values equal to 18.31%, 23.34%, and 26.15%. The influence of plant density on the performance of LR-CC was also evaluated by the three density datasets. Each density dataset containing 16 observations was used for test. Linear regression was used as a statistical prediction model between the CC values and AGB (Fig.13). The R² values of the model over three density datasets were 0.8129, 0.7775 and 0.7183, respectively, the RMSE values were 0.6243, 0.8517, and 1.2212 kg/plot, respectively, and the NRMSE values were 28.48%, 33.03%, and 43.41%, respectively. (Table 5).

For the three conventional classifiers on the density datasets, the performances were shown in Fig. 14. Similar results to LR-CC can be observed (Table 5).

Table 5 presented the evaluation results of all the estimation methods on the density datasets. The DCNN still outperformed the other methods on the density datasets.

3.3. Results on the temporal dataset

The influence of temporal information of the field measured AGB on different DAS on the estimated AGB was evaluated. Canopy images captured on five DAS (DAS093, DAS115, DAS138, DAS146, and DAS153) were deducted for training. Therefore, the training of the DCNN was not using the information presented by canopy images captured on these five DAS. Canopy images captured on the other 12 DAS were used to construct the datasets for training and validation. Data augmentation was performed to all the datasets. According to this experiment setup, a temporal dataset was constructed and the number of images in the three datasets was 8985, 2247, 4680 respectively. The estimates of AGB for each plot were computed by averaging the three estimated values from the marker images within the plot. The performance of the DCNN evaluated over the test dataset was shown in Fig.15.

Although the performance slightly decreased (R² = 0.7629, RMSE = 0.9409 kg/plot, NRMSE = 23.87%), the DCNN was still capable of giving accurate AGB estimations. The influence of temporal information on the performances of the compared methods was also evaluated. To obtain the results, the compared methods were trained on

Table 2
Estimation results of the DCNN under the influences of different factors.

Factors	Range						
Number of input images							
Methods	No augmentation	Rotation + flip	Flip + illumination adjustment	Rotation + illumination adjustment	Rotation + flip + illumination adjustment	/	/
Number of training images	408	2448	4488	6528	10608	/	/
R ²	0.2284	0.4251	0.5414	0.7062	0.808	/	/
RMSE (Kg/plot)	1.9646	1.506	1.3169	1.1081	0.8913	/	/
NRMSE (%)	56.38%	52.31%	42.45%	32.15%	24.95%	/	/
Learning rate							
Range	10 ⁻³	10 ⁻⁴	10 ⁻⁵	10 ⁻⁶	10 ⁻⁷	10 ⁻⁸	Dynamic
R ²	0.707	0.7292	0.7616	0.7002	0.6739	0.671	0.808
RMSE (Kg/plot)	0.8049	0.9206	0.8695	0.9891	1.0109	0.7648	0.8913
NRMSE (%)	21.08%	26.96%	25.64%	28.46%	30.12%	79.43%	24.95%
Mini-batch size							
Range	8	16	32	64	128	256	/
R ²	0.3667	0.523	0.749	0.808	0.7177	0.6763	/
RMSE (Kg/plot)	0.5252	0.5360	0.8619	0.8913	1.0534	1.1991	/
NRMSE (%)	14.48%	15.59%	24.41%	24.95%	30.87%	34.98%	/

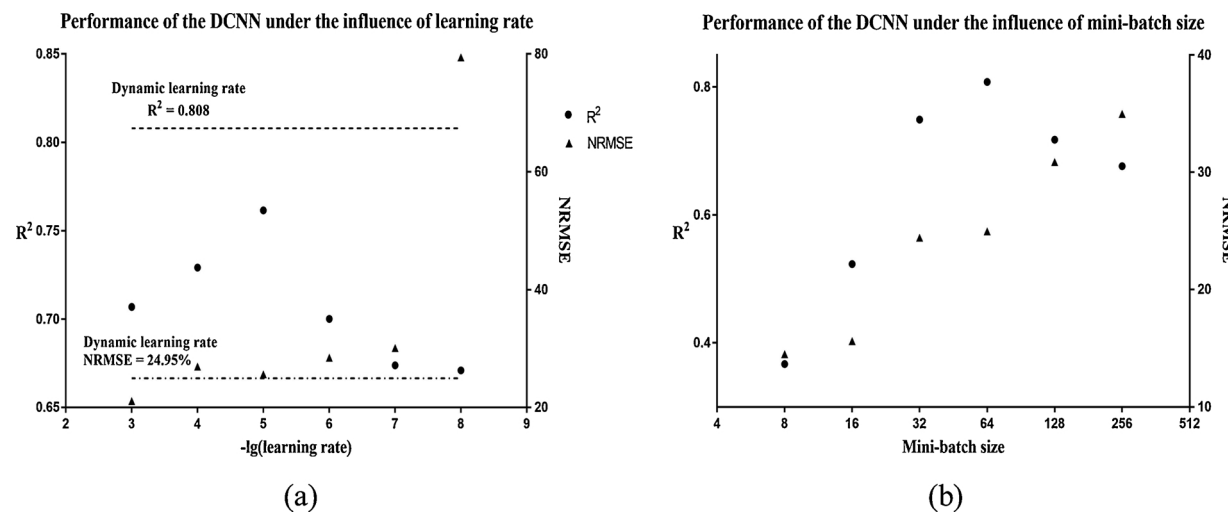


Fig. 8. Performance of the DCNN under the influence of different factors, (a) learning rate, (b) mini-batch size.

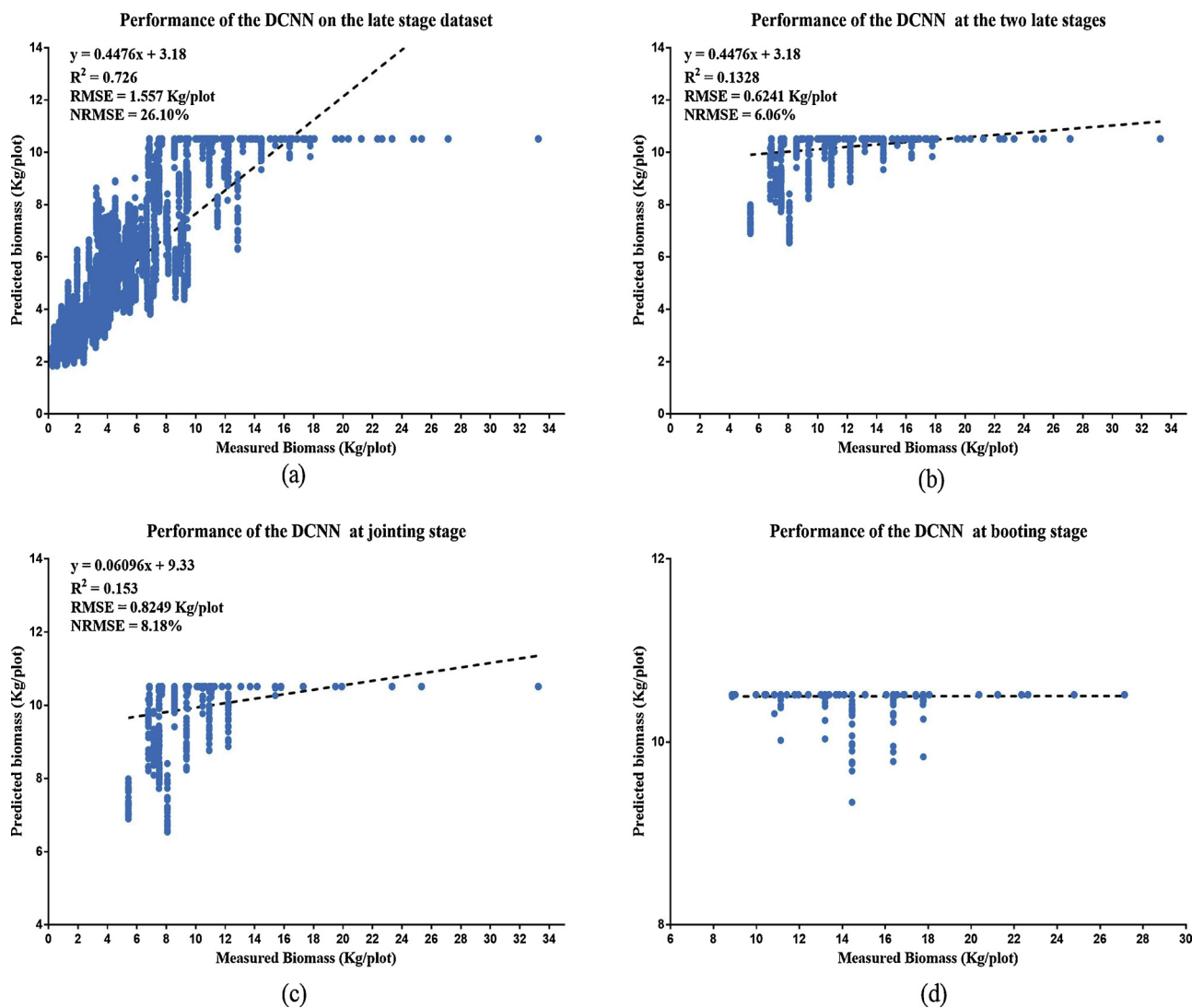


Fig. 9. Performance of the DCNN at late growth stages, (a) early stage and the two late stages, (b) the two late stages, (c) jointing stage, (d) booting stage.

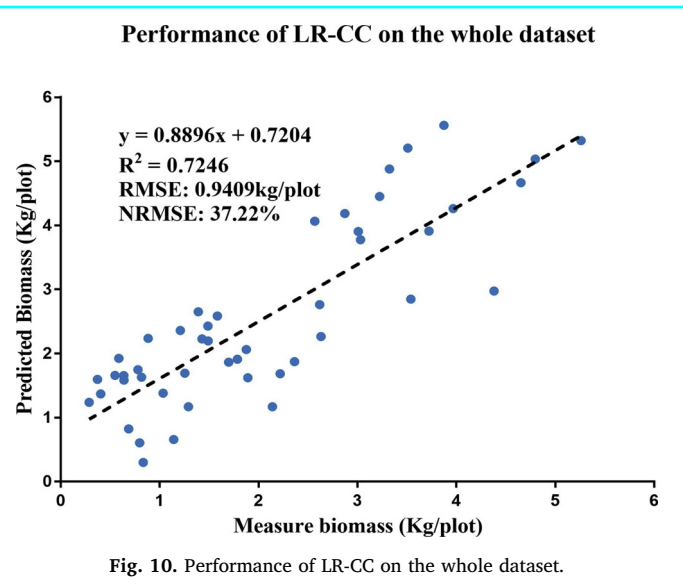


Fig. 10. Performance of LR-CC on the whole dataset.

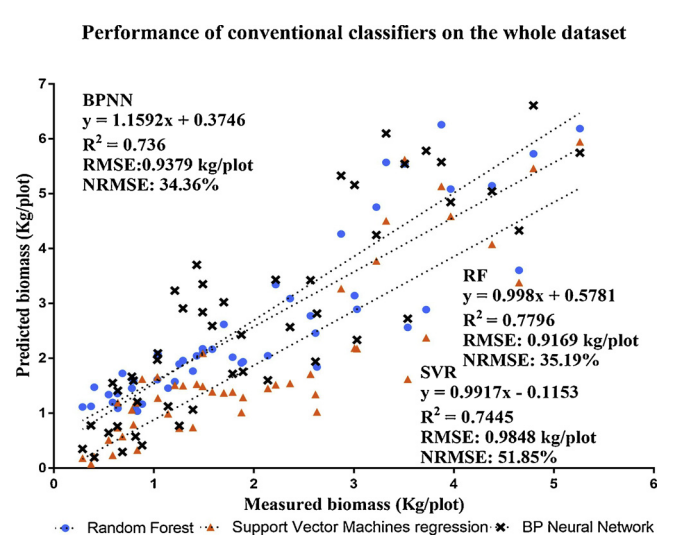


Fig. 11. Performance of conventional classifiers on the whole dataset.

144 observations (4 plots \times 3 densities \times 12 times) and tested on 48 observations (4 plots \times 3 densities \times 4 times) of the left-out DAS. 12 observations on DAS 115 were removed as outliers. The estimation results were shown in Fig. 16.

Table 6 presented the evaluation results of all the methods under the influence of temporal information. It can be seen the DCNN consistently outperformed the compared methods over the temporal dataset.

4. Discussion

Convolutional neural network (CNN) is currently the state-of-the-art technique for image processing (Ghosal et al., 2018; LeCun et al., 2015). As opposed to the conventional shallow machine learning method, CNN can automatically learn appropriate features from training datasets instead of manual feature extraction (Ferreira et al., 2017; LeCun et al., 2015), achieving promising results in a wide range of plant phenotyping tasks, such as plant stress phenotyping (Ghosal et al., 2018), weed detection (Ferreira et al., 2017), plant disease recognition (Ferentinos, 2018; Ma et al., 2018; Mohanty et al., 2016), and plant species identification (Krause et al., 2018; Grinblat et al., 2016). The results obtained from this research indicated the potentials of the DCNN in estimating AGB. Compare to the four methods, the DCNN was

Table 4
AGB estimation results on the whole dataset.

Evaluation metrics	Methods				
	DCNN	LR-CC	RF	SVR	BPNN
R^2	0.808	0.7246	0.7796	0.7445	0.736
RMSE (kg/plot)	0.8913	0.9409	0.9169	0.9848	0.9379
NRMSE (%)	24.95%	37.22%	35.19%	51.85%	34.36%

a more direct method for AGB estimation. The image segmentation of vegetation was not necessary because the DCNN was able to use the important features to estimate AGB and ignore the non-important features, which not only reduced the computation cost but also increased the efficiency of the estimation (Ferentinos, 2018). In contrast, the performances of the compared estimating methods greatly depended on the results of image segmentation. Accurate segmentation results guaranteed accurate data sources to feature extraction. However, canopy images captured under real field conditions were suffering from uneven illumination and complicated background, which was a big challenge to achieve robust image segmentation of vegetation. (Ma et al., 2017).

Table 3
Correlations of the AGB measurements with the features.

Above ground biomass									
R_avg	.470**	h_avg	.478**	l_avg	.530**	y_avg	.523**	H_avg	.155*
R_std	-.053	h_std	-.681**	l_std	.016	y_std	.054	H_std	-.657**
R_Contrast	.209**	h_Contrast	-.650**	l_Contrast	-.543**	y_Contrast	.181**	H_Contrast	-.576**
R_Correlation	-.200**	h_Correlation	-.555**	l_Correlation	-.678**	y_Correlation	-.170*	H_Correlation	-.240**
R_Energy	-.554**	h_Energy	.659**	l_Energy	.644**	y_Energy	-.572**	H_Energy	.556*
R_Homogeneity	-.616**	h_Homogeneity	.541**	l_Homogeneity	.532**	y_Homogeneity	-.620**	H_Homogeneity	.531**
G_avg	.539**	s_avg	.181**	a_avg	-.568**	cb_avg	-.382**	S_avg	-.599**
G_std	.094	s_std	-.584**	a_std	.386*	cb_std	.185*	S_std	-.504**
G_Contrast	.242**	s_Contrast	-.430**	a_Contrast	-.541**	cb_Contrast	-.349**	S_Contrast	-.284**
G_Correlation	-.077	s_Correlation	-.093	a_Correlation	-.571**	cb_Correlation	-.604**	S_Correlation	-.188**
G_Energy	-.572**	s_Energy	-.461**	a_Energy	.669**	cb_Energy	.594**	S_Energy	-.487**
G_Homogeneity	-.625**	s_Homogeneity	-.431**	a_Homogeneity	.656**	cb_Homogeneity	.349**	S_Homogeneity	-.416**
B_avg	.499**	v_avg	.538**	b_avg	.423**	cr_avg	-.588**	I_avg	.515**
B_std	.249**	v_std	.102	b_std	.187**	cr_std	.459**	I_std	.083
B_Contrast	.317**	v_Contrast	.242**	b_Contrast	-.456**	cr_Contrast	-.528**	I_Contrast	.265**
B_Correlation	-.062	v_Correlation	-.077	b_Correlation	-.734**	cr_Correlation	-.627**	I_Correlation	-.142*
B_Energy	-.553**	v_Energy	-.572**	b_Energy	.602**	cr_Energy	.667**	I_Energy	-.563**
B_Homogeneity	-.624**	v_Homogeneity	-.625**	b_Homogeneity	.434**	cr_Homogeneity	.528**	I_Homogeneity	-.623**

* Correlation is significant at the 0.05 level.

** Correlation is significant at the 0.01 level.

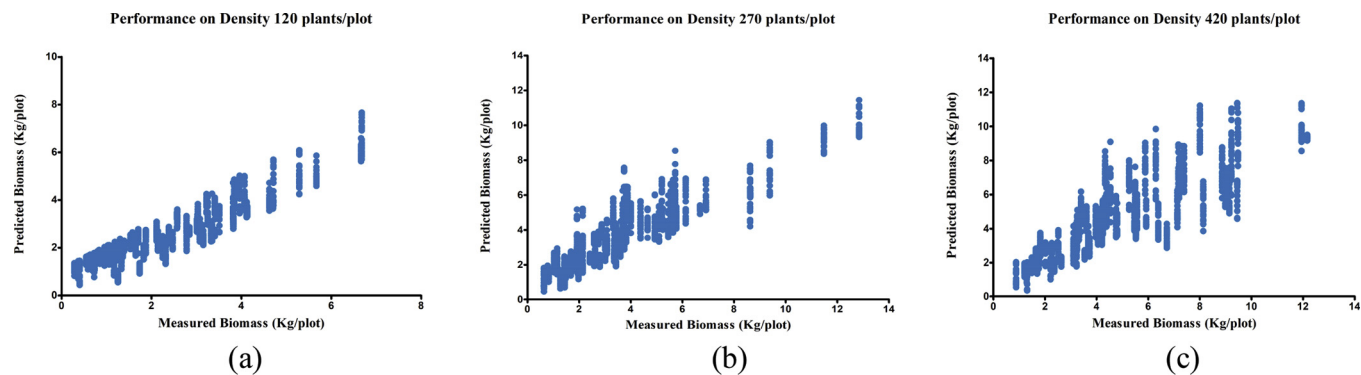


Fig. 12. Performance of the DCNN on the density datasets, (a) Density 120, (b) Density 270, (c) Density 420.

Table 5
AGB estimation results under influence of plant density.

Evaluation metrics	Datasets	Methods				
		DCNN	LR-CC	RF	SVR	BPNN
R ²	Density 120	0.8693	0.8129	0.8314	0.7952	0.8261
	Density 270	0.8062	0.7775	0.7628	0.7146	0.6995
	Density 420	0.7433	0.7183	0.6887	0.6575	0.6124
RMSE (Kg/plot)	Density 120	0.4796	0.6243	0.5597	0.7061	0.6655
	Density 270	0.8495	0.8517	0.8526	0.8949	0.8949
	Density 420	1.1656	1.2212	1.2972	1.2876	1.1797
NRMSE (%)	Density 120	18.31%	28.48%	26.78%	58.38%	39.24%
	Density 270	23.34%	33.03%	28.66%	36.66%	24.73%
	Density 420	26.15%	43.41%	49.35%	62.87%	41.04%

The number of images in the input dataset was proved to be an influence of factor to the DCNN, which agreed with the conclusion that the DCNN can achieve satisfactory results with a large number of input images (Ferreira et al., 2017; Ma et al., 2018). It can be seen in Table 2 that the DCNN demonstrated an improving trend with the increase of the number of training images. Compared to no augmentation, all the augmentation schemes improved the performance of the DCNN. The best performance was achieved by the DCNN on dataset rotation + flip + illumination adjustment augmentation. The results indicated that data augmentation was necessary to the DCNN on AGB estimation, which can enlarge the number of input dataset, as well as enable the input dataset to cover as much variability as in the field conditions.

As it was shown in Table 1, the performances of the DCNN over the whole dataset were consistently superior to that over the gray whole dataset on each measured date, indicating that the color information of canopy images was also an influence of factor to the DCNN. Color information was essential to discriminate canopy and soil, therefore, the removal of the color information from the gray whole dataset disabled the DCNN to discriminate canopy and soil, leading to an obvious

decrease on the performance of the DCNN over the gray whole dataset. The results indicated that the color information was necessary to AGB estimation by using digital images and DCNN. Learning rate and mini-batch size were two factors that influenced the accuracy of DCNN for AGB estimation. Both two factors had second-order effects on the performance of the DCNN (Fig. 8a, b). According to the experiments, dynamic learning rate and a mini-batch size of 64 was suitable for the DCNN in this study to estimate AGB. It can be seen in Fig. 9 that the DCNN in this study was not able to estimate AGB at late growth stages. The estimation results for the two late growth stages were much worse than those for the early stages. Especially for the booting stage, the estimation results were seemed to reach the upper limit, staying around 10 kg/plot even though the winter wheat was gaining dry matters. This upper limit may be rooted in the input layer, whose input images with size $64 \times 64 \times 3$ were not informative enough for the DCNN to capture the canopy details at late growth stages. Therefore, it was suggested to use input images of higher resolution for the DCNN to estimate AGB at late growth stages.

It can be seen from Table 5 that a noticeable drop in the performances of the compared methods can be observed when the plant density increased from 120 to 420 plants/m² while the DCNN only slightly dropped from 0.8693 to 0.7433, indicating that the plant density influenced the performance of the conventional classifiers while the DCNN made a robust tool to estimate AGB of winter wheat at early growth stages. Linear regression model using CC as the predictor variable could achieve good estimations of AGB in a relatively low-density plot, which agreed with several previous studies on using CC to estimate the growth-related traits (Casadesús and Villegas, 2014; Rahaman et al., 2015; Gizaw et al., 2016; Naito et al., 2017). In the relatively low-density plot, the adjacent leaves barely overlapped. The information presented by the vegetation can be fully captured by digital images. In the relatively high-density plot, the overlapping adjacent leaves caused missing information of the green structure in the digital images. The reason why the DCNN consistently outperformed the compared

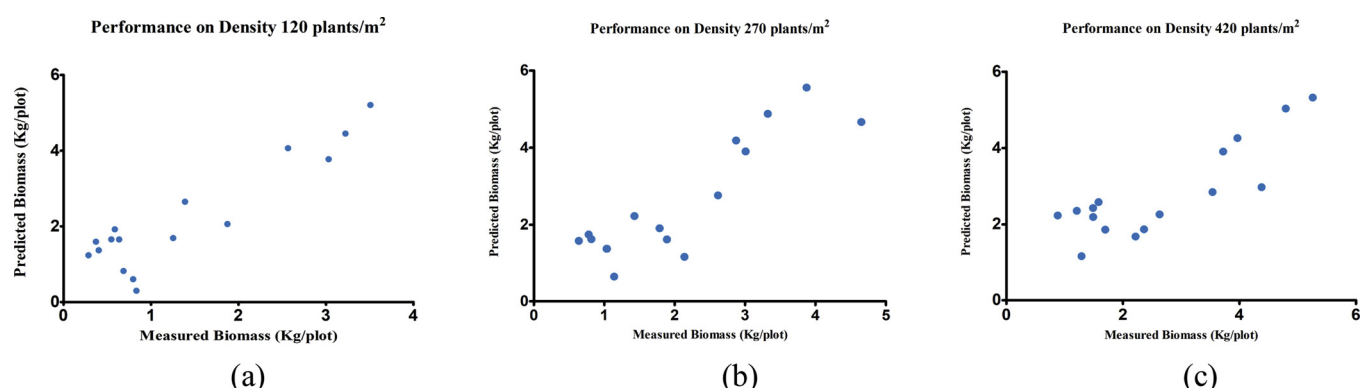


Fig. 13. Performance of LR-CC on the density datasets, (a) Density 120, (b) Density 270, (c) Density 420.

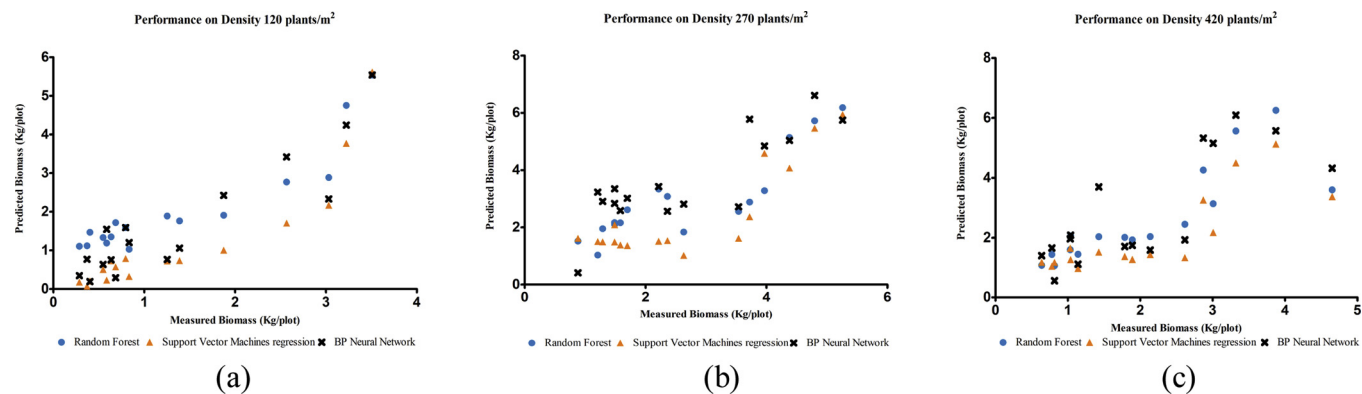


Fig. 14. Performance of the conventional classifiers on the density datasets, (a) Density 120, (b) Density 270, (c) Density 420.

Performance of the DCNN under the influence of temporal information

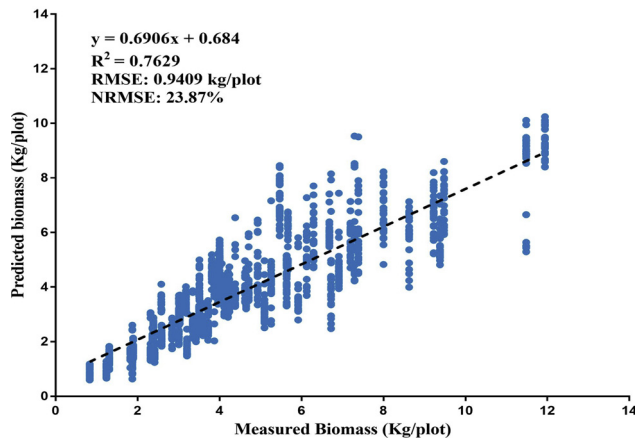


Fig. 15. Performance of the DCNN under the influence of temporal information.

methods over the temporal dataset was that the quality of the image features was a determinant factor in the performance of the compared methods. For these methods, low-level features were manually designed, resulting in the weak generalization ability to AGB estimation.

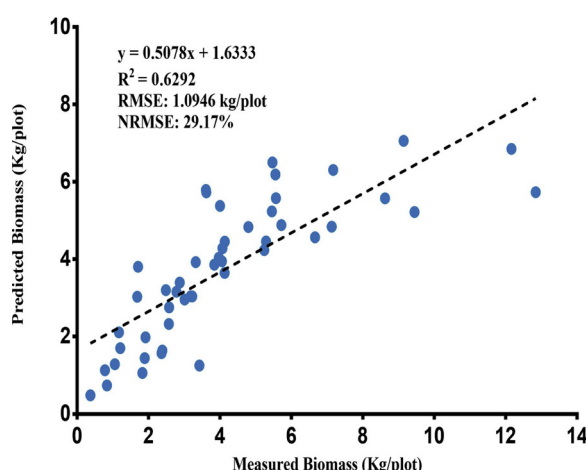
Table 6
AGB estimation results under influence of temporal information.

Evaluation metrics	Methods				
	DCNN	LR-CC	RF	SVR	BPNN
R^2	0.7629	0.6292	0.6994	0.6818	0.6443
RMSE (kg/plot)	0.9409	1.0946	1.0877	1.2034	1.2387
NRMSE (%)	23.87%	29.17%	27.53%	30.53%	32.30%

In contrast, the DCNN can automatically learn appropriate features from canopy images of winter wheat instead of manual feature design, which turned out to be a reliable tool for AGB estimation.

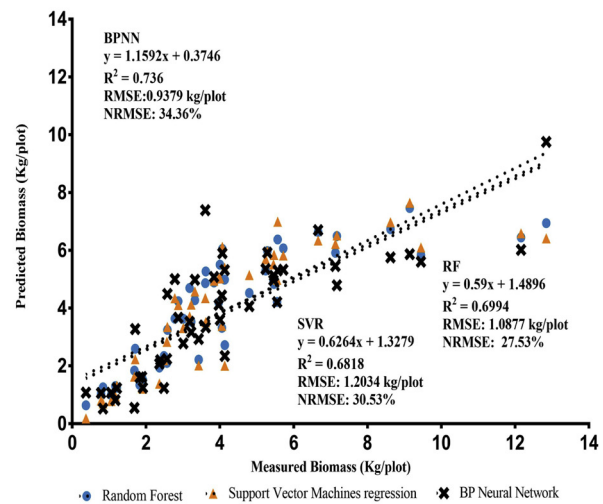
In this study, an easy-to-use AGB estimation method for winter wheat at early growth stages was proposed by using digital images captured under field conditions and deep convolutional neural network. The method was performed on digital images of three density datasets ($120, 270$ and 420 plants/ m^2). The results showed that the performance dropped with the increase of plant density. One possible reason for the drop was that the canopy structure information could not be captured by digital images. With the increase of plant density, adjacent leaves overlapped, resulting in structure information that was inaccessible by digital cameras oriented towards nadir. To make the method robust to the variation of plant density, one possible way was to adopt the 3D

Performance of LR-CC under the influence of temporal information



(a)

Performance of conventional classifiers under the influence of temporal information



(b)

Fig. 16. Performance of compared methods under the influence of temporal information, (a) LR-CC, (b) conventional classifiers.

information of the canopy. Point clouds created by LiDAR (Eitel et al., 2014; Greaves et al., 2015) or Photogrammetry (Walter et al., 2018) were widely adopted to utilize the 3D information for AGB estimation. Predictors derived from point clouds were strongly correlated with AGB. Although point cloud showed good potential to estimate AGB, there existed limitations that the creation of point cloud required high-cost device and heavy calculation cost. Therefore, low-cost solutions, such as depth images, can alternatively help the DCNN to maintain robustness to plant density.

5. Conclusion

An AGB estimation method for winter wheat at early growth stages based on the DCNN was proposed in this paper. The method took RGB images of winter wheat canopy captured by a low-cost digital camera as input. The estimated AGB values showed strong correlations to manual measurements ($R^2 = 0.808$), indicating the potential of the DCNN for estimating growth-related traits. The performance of DCNN was compared to the conventional methods adopted to estimate AGB. Image datasets with different plant densities (120, 270 and 420 plants/m²) and temporal influence were constructed to test the methods. Results showed the performances of all the methods were influenced to varying degrees by plant density while the DCNN achieved the best robustness. Experiment on temporal influence showed the DCNN had a good generalization ability. Color information of canopy images and the number of training images were the influence of factors to the DCNN. To achieve robust estimation results, it was necessary to use a considerable number of RGB images for the DCNN. Learning rate and mini-batch size were two factors that could influence the accuracy of DCNN for AGB estimation as well. It was suggested to do parameter search to find the suitable values for the DCNN. Experiments indicated that the DCNN in this study was not capable of estimating AGB at late growth stages due to the limited details of the canopy presented by the relatively small size images of the input layer. It was suggested to use images of higher resolution for the DCNN to estimate AGB at late growth stages.

Since the DCNN makes a reliable tool for AGB estimation, there is a good chance that the method is extended to high-throughput phenotyping use by combining with mobile devices. Canopy images can be captured by cameras on the mobile devices and transferred to the server side where a pre-trained DCNN network was stored. Once the network gave the estimation result, it could be transferred back to the mobile devices to be demonstrated to users. Moreover, the DCNN can be integrated into the high-throughput phenotyping platforms since its input images can be captured by low-cost digital cameras. The AGB estimation results showed that the DCNN had a good potential for the estimation of the growth-related traits. The same technique used in AGB estimation for winter wheat can be applied to other growth-related traits by modifying the datasets, as well as to different types of crop. In order to improve the efficiency, an automatic image processing method for detecting the markers will be developed in the future work.

Acknowledgments

The Authors wish to acknowledge The National Key Research and Development Program of China (2016YFD0300606), The National Natural Science Foundation of China (31801264) and The National Key Research and Development Program of China (2017YFD0300401) for their funding support of this research.

References

- Bai, G., Ge, Y., Hussain, W., Baenziger, P.S., Graef, G., 2016. A multi-sensor system for high throughput field phenotyping in soybean and wheat breeding. *Comput. Electron. Agric.* 128, 181–192.
- Baresel, J.P., Rischbeck, P., Hu, Y., Kipp, S., Hu, Y., Barneier, G., Mistele, B., 2017. Use of a digital camera as alternative method for non-destructive detection of the leaf chlorophyll content and the nitrogen nutrition status in wheat. *Comput. Electron. Agric.* 140, 25–33.
- Bendig, J., Yu, K., Asen, H., Bolten, A., Bennertz, S., Broscheit, J., Gnyp, M.L., Bareth, G., 2015. Combining UAV-based plant height from crop surface models, visible, and near infrared vegetation indices for biomass monitoring in barley. *Int. J. Appl. Earth Obs. Geoinf.*
- Breiman, L., 2001. Random forests. *Mach. Learn.* 45 (1), 5–32.
- Casadesús, J., Villegas, D., 2014. Conventional digital cameras as a tool for assessing leaf area index and biomass for cereal breeding. *J. Integr. Plant Biol.* 56, 7–14.
- Chang, Y.K., Zaman, Q.U., Rehman, T.U., Farooque, A.A., Esau, T., Jameel, M.W., 2017. A real-time ultrasonic system to measure wild blueberry plant height during harvesting. *Biosyst. Eng.* 157, 35–44.
- Chung, Y.S., Choi, S.C., Silva, R.R., Kang, J.W., Eom, J.H., Kim, C., 2017. Case study: estimation of sorghum biomass using digital image analysis with Canopeo. *Biomass Bioenergy* 105, 207–210.
- Clevers, J.G.P.W., van der Heijden, G.W.A.M., Verzakov, S., Schaepman, M.E., 2007. Estimating grassland biomass using svm band shaving of hyperspectral data. *Photogramm. Eng. Rem. Sens.* 73 (10), 1141–1148.
- Daughtry, C.S.T., Walthal, C.L., Kim, M.S., de Colstoun, E.B., McMurtrey, J.E., 2000. Estimating corn leaf chlorophyll concentration from leaf and canopy reflectance. *Remote Sens. Environ.* 74, 229–239.
- Ding, W., Taylor, G., 2016. Automatic moth detection from trap images for pest management. *Comput. Electron. Agric.* 123, 17–28.
- Eitel, J.U.H., Magney, T.S., Vierling, L.A., Brown, T.T., Huggins, D.R., 2014. LiDAR based biomass and crop nitrogen estimates for rapid, non-destructive assessment of wheat nitrogen status. *Field Crop. Res.* 159, 21–32.
- Fan, X., Kawamura, K., Guo, W., Xuan, T.D., Lim, J., Yuba, N., Kurokawa, Y., Obitsu, T., Lv, R., Tsumiyama, Y., Yasuda, T., Wang, Z., 2017. A simple visible and near-infrared (V-NIR) camera system for monitoring the leaf area index and growth stage of Italian ryegrass. *Comput. Electron. Agric.* 1–10.
- Ferentinos, K.P., 2018. Deep learning models for plant disease detection and diagnosis. *Comput. Electron. Agric.* 145, 311–318.
- Ferreira, A.D.S., Freitas, D.M., Silva, G.G.D., Pistori, H., Folhes, M.T., 2017. Weed detection in soybean crops using convnets. *Comput. Electron. Agric.* 143, 314–324.
- Ghosal, S., Blystone, D., Singh, A.K., Ganapathysubramanian, B., Singh, A., 2018. An explainable deep machine vision framework for plant stress phenotyping. *Proc. Natl. Acad. Sci. U. S. A.* 1–6.
- Gizaw, S.A., Garland-Campbell, K., Carter, A.H., 2016. Use of spectral reflectance for indirect selection of yield potential and stability in Pacific Northwest winter wheat. *Field Crop. Res.* 196, 199–206.
- Gnyp, M.L., Bareth, G., Li, F., Lenz-Wiedemann, V.I.S., Koppe, W., Miao, Y., Hennig, S.D., Jia, L., Laudien, R., Chen, X., Zhang, F., 2014. Development and implementation of a multiscale biomass model using hyperspectral vegetation indices for winter wheat in the North China Plain. *Int. J. Appl. Earth Obs. Geoinf.*
- Greaves, H.E., Vierling, L.A., Eitel, J.U.H., Boelman, N.T., Magney, T.S., Prager, C.M., Griffin, K.L., 2015. Estimating aboveground biomass and leaf area of low-stature Arctic shrubs with terrestrial LiDAR. *Remote Sens. Environ.* 164, 26–35.
- Grinblat, G.L., Uzal, L.C., Larese, M.G., Granitto, P.M., 2016. Deep learning for plant identification using vein morphological patterns. *Comput. Electron. Agric.* 127, 418–424.
- Jannoura, R., Brinkmann, K., Uteau, D., Bruns, C., Joergensen, R.G., 2015. Monitoring of crop biomass using true colour aerial photographs taken from a remote controlled hexacopter. *Biosyst. Eng.* 129, 341–351.
- Jiang, Y., Li, C., Paterson, A.H., 2016. High throughput phenotyping of cotton plant height using depth images under field conditions. *Comput. Electron. Agric.* 130, 57–68.
- Krause, J., Sugita, G., Baek, K., Lim, L., 2018. WTPPlant (what's that plant?): A deep learning system for identifying plants in natural images. *Proceedings of the 2018 ACM on International Conference on Multimedia Retrieval - ICMR' 18.* pp. 517–520.
- Krizhevsky, A., Sutskever, I., Hinton, G.E., 2012. ImageNet classification with deep convolutional neural networks. *Adv. Neural Inf. Process. Syst.* 1–9.
- LeCun, Y., Bengio, Y., Hinton, G., 2015. Deep learning. *Nature* 521 (7553), 436–444.
- Liebisch, F., Kirchgessner, N., Schneider, D., Walter, A., Hund, A., 2015. Remote, aerial phenotyping of maize traits with a mobile multi-sensor approach. *Plant Methods* 11.
- Ma, J., Du, K., Zhang, L., Zheng, F., Chu, J., Sun, Z., 2017. A segmentation method for greenhouse vegetable foliar disease spots images using color information and region growing. *Comput. Electron. Agric.* 142, 110–117.
- Ma, J., Du, K., Zheng, F., Zhang, L., Gong, Z., Sun, Z., 2018. A recognition method for cucumber diseases using leaf symptom images based on deep convolutional neural network. *Comput. Electron. Agric.* 154, 18–24.
- Moeckel, T., Safari, H., Reddersen, B., Fricke, T., Wachendorf, M., 2017. Fusion of ultrasonic and spectral sensor data for improving the estimation of biomass in grasslands with heterogeneous sward structure. *Remote Sens.* 9, 1–14.
- Mohanty, S.P., Hughes, D., Salathe, M., 2016. Inference of Plant Diseases from Leaf Images Through Deep Learning. *arXiv1604.03169 [cs].* pp. 1–6.
- Naito, H., Ogawa, S., Valencia, M.O., Mohri, H., Urano, Y., Hosoi, F., Shimizu, Y., Chavez, A.L., Ishitani, M., Selvaraj, M.G., Omasa, K., 2017. Estimating rice yield related traits and quantitative trait loci analysis under different nitrogen treatments using a simple tower-based field phenotyping system with modified single-lens reflex cameras. *ISPRS J. Photogramm. Remote Sens.* 125, 50–62.
- Patrignani, A., Ochsner, T.E., 2015. Canopeo: a powerful new tool for measuring fractional green canopy cover. *Agron. J.* 107, 2312–2320.
- Pittman, J.J., Arnall, D.B., Interrante, S.M., Moffet, C.A., Butler, T.J., 2015. Estimation of biomass and canopy height in Bermudagrass, Alfalfa, and wheat using ultrasonic, laser, and spectral sensors. *Sensors (Switzerland)* 15, 2920–2943.
- Pöllönen, I., Saari, H., Kaivosoja, J., Honkavaara, E., Pesonen, L., 2013. Hyperspectral imaging based biomass and nitrogen content estimations from light-weight UAV.

- Proc. SPIE Int. Soc. Opt. Eng. 888, 521–525.
- Possoch, M., Bieker, S., Hoffmeister, D., Bolten, A., Schellberg, J., Bareth, G., Conservation, R., Group, C.S., Conservation, R., Ecology, P., Model, C.S., 2016. Multi-temporal crop surface models combined with the RGB vegetation index from UAV-based images for forage monitoring in grassland. *ISPRS Int. Arch. Photogramm. Remote Sens. Spat. Inf. Sci.* XLI, 12–19.
- Rahaman, M.M., Chen, D., Gillani, Z., Klukas, C., Chen, M., 2015. Advanced phenotyping and phenotype data analysis for the study of plant growth and development. *Front. Plant Sci.* 6, 1–15.
- Rasmussen, J., Ntakos, G., Nielsen, J., Svensgaard, J., Poulsen, R.N., Christensen, S., 2016. Are vegetation indices derived from consumer-grade cameras mounted on UAVs sufficiently reliable for assessing experimental plots? *Eur. J. Agron.* 74, 75–92.
- Rischbeck, P., Elsayed, S., Mistele, B., Barneier, G., Heil, K., Schmidhalter, U., 2016. Data fusion of spectral, thermal and canopy height parameters for improved yield prediction of drought stressed spring barley. *Eur. J. Agron.* 78, 44–59.
- Schirrmann, M., Giebel, A., Gleiniger, F., Pflanz, M., Lentschke, J., Dammer, K.H., 2016a. Monitoring agronomical parameters of winter wheat crops with low-cost UAV imagery. *Remote Sens.* 8, 706.
- Schirrmann, M., Hamdorf, A., Garz, A., Ustyuzhanin, A., Dammer, K.H., 2016b. Estimating wheat biomass by combining image clustering with crop height. *Comput. Electron. Agric.* 121, 374–384.
- Simonyan, K., Zisserman, A., 2014. Very Deep Convolutional Networks for Large-Scale Image Recognition. arXiv preprint arXiv:1409.1556. .
- Tucker, C.J., 1979. Asymptotic nature of grass canopy spectral reflectance. *Appl. Opt.* 16, 1151–1156.
- Tucker, C.J., 1979. Red and photographic infrared linear combinations for monitoring vegetation. *Remote Sens. Environ.* 8, 127–150.
- Walter, J., Edwards, J., McDonald, G., Kuchel, H., 2018. Photogrammetry for the estimation of wheat biomass and harvest index. *Field Crop. Res.* 216, 165–174.
- Wang, L., Zhou, X., Zhu, X., Dong, Z., Guo, W., 2016. Estimation of biomass in wheat using random forest regression algorithm and remote sensing data. *Crop J.* 4, 212–219.
- Woebbecke, D.M., Meyer, G.E., Von Bargen, K., Mortensen, D.A., 1995. Color indices for weed identification under various soil, residue, and lighting conditions. *Trans. Am. Soc. Agric. Eng.* 38, 259–269.
- Xiong, X., Duan, L., Liu, L., Tu, H., Yang, P., Wu, D., Chen, G., Xiong, L., Yang, W., Liu, Q., 2017. Panicle-SEG: a robust image segmentation method for rice panicles in the field based on deep learning and superpixel optimization. *Plant Methods* 13, 1–15.
- Zhang, L., Verma, B., Stockwell, D., Chowdhury, S., 2018. Density weighted connectivity of grass pixels in image frames for biomass estimation. *Expert Syst. Appl.* 101, 213–227.